Effects of the lanthanide addition to the Sr_2CrReO_6 double perovskite

J. Blasco,[1,*] J. M. Michalik,[1,2] J. García,[1] G. Subías,[1] and J. M. De Teresa[1]

[1]*Instituto de Ciencia de Materiales de Aragón and Departamento de Física de la Materia Condensada, Consejo Superior de Investigaciones Científicas y Universidad de Zaragoza, 50009 Zaragoza, Spain*

[2]*Department of Solid State Physics, Faculty of Physics and Applied Computer Sciences, AGH University of Science and Technology, 30-059 Cracow, Poland*

(Received 15 March 2007; revised manuscript received 28 August 2007; published 1 October 2007)

We have studied the effects of Sr replacement by different lanthanides in Sr_2CrReO_6. Our attempts at electron doping of Sr_2CrReO_6 led to multiphasic systems. Single phases are only obtained with the stoichiometric formula $Sr_{2-x}Ln_xCr_{1+x/2}Re_{1-x/2}O_6$. We have studied the properties of these compounds with $x \leqslant 0.5$ and Ln=La, Nd, or Sm. All of these samples crystallize in a face-centered cubic cell, which shrinks as Ln-size decreases. The distribution of Re and Cr atoms has been solved using x-ray diffraction. The samples show spontaneous magnetization at room temperature with large coercive fields. The Ln addition slightly affects the Curie temperature although the saturated magnetic moment decreases, owing to the increase of antisite defects. We have also studied $Sr_{2-x}Nd_xCr_{1+x/2}Re_{1-x/2}O_6$ and $Sr_{2-x}Sm_xCr_{1+x/2}Re_{1-x/2}O_6$ ($x \leqslant 0.5$) by means of x-ray absorption spectroscopy. The spectra at the Cr *K* edge agree with the presence of Cr^{3+} for all compounds although changes with increasing the rare-earth content are visible at the preedge features. These changes suggest a change in the Cr-O covalency of the samples with increasing Ln content. Measurements at the Re $L_{1,2,3}$ edges reveal the presence of Re^{5+} in all compounds. This implies that replacing Sr by Ln does not affect the electronic state of both Cr^{3+} and Re^{5+}.

DOI: 10.1103/PhysRevB.76.144402 PACS number(s): 75.50.Gg, 61.10.Ht, 78.70.Dm, 61.10.Nz

I. INTRODUCTION

There is much interest in the study of ferromagnetic oxides with a Curie temperature (T_C) well above room temperature and with a high spin polarization of the conduction electrons.[1–4] Such materials are potentially useful for applications in magnetoelectronic devices. There are several members belonging to the so-called double perovskite (DP) family namely, Re- and Mo-based compounds, exhibiting a half-metallic ground state and a high T_C.[1] Among them, Sr_2CrReO_6 has one of the highest T_C and a large conductivity.[2] One successful route to further increase T_C in Mo-based DP was via electron doping, i.e., partial substitution of Sr with rare-earth (Ln) in order to fill the $4d$ t_{2g} minority spin band.[3] In this way, T_C was increased to more than 100 K for one doped electron per unit cell in the $Sr_{2-x}La_xFeMoO_6$ series.[3]

However, this strategy failed to increase T_C in Sr_2CrReO_6 through Nd^{3+} doping ($Sr_{2-x}Nd_xCrReO_6$) as these compounds showed equal or lower T_C together with an increase of the electrical resistivity.[4] This result is even more amazing, taking into account that Sr_2CrOsO_6 with a completely filled $5d$ t_{2g} minority band shows the highest T_C among these compounds.[5] The presence of secondary phases in the preparation of $Sr_{2-x}Ln_xCrReO_6$ could throw doubts on the actual atomic stoichiometry for the main phase. In order to shed light on this subject, an accurate structural study is needed to overcome the current lack of knowledge about the phase diagram in the La-Sr-Cr-Re-O system and the possibility of the existence of effective electron doping. With this aim, we have developed the present study of the crystal and electronic structures for a wide set of double perovskites with nominal composition ranging between $Sr_{2-x}Ln_xCrReO_6$ and $Sr_{2-x}Ln_xCr_{1+x/2}Re_{1-x/2}O_6$ (Ln=La, Nd, and Sm).

In order to determine the extent of doping, a local technique is needed to independently determine the electronic change on both Re and Cr atoms. For such studies, x-ray absorption spectroscopy has proven to be a powerful technique to obtain information about the electronic structure and local geometry around different absorbing atoms in many systems.[6] In this survey, we have measured the x-ray absorption near edge structure (XANES) and extended x-ray absorption fine structure (EXAFS) spectra of Ln-based DP at both the Cr *K* and Re *L* edges. Unfortunately, the coincidence of La *L* and Cr *K* edges prevented us from studying La-based samples and, for the same reason, the study was limited to the XANES spectroscopy for the Nd-based samples. However, XANES and EXAFS spectra can be recorded for the Sm-based samples, allowing us to extrapolate our conclusions to the rest of the series due to the fact that the rare-earth size had minor effects on the structural properties of these compounds as can be seen later.

II. EXPERIMENTAL

Polycrystalline $Sr_{2-x}Ln_xCrReO_6$ and $Sr_{2-x}Ln_xCr_{1+x/2}Re_{1-x/2}O_6$ samples ($x=0$, 0.1, 0.3, and 0.5; Ln=La, Nd or Sm) were prepared by solid-state reaction.[7] Stoichiometric amounts of $SrCO_3$, Ln_2O_3, Cr_2O_3, ReO_3, and Re (ReO_3/Re ratio is 5/1) were mixed and pressed into pellets. The pellets were heated at 1375 °C for 2 h in a gas flow of Ar/H_2 (ratio of 99.9/0.1). This process was repeated several times up to the end of the chemical reaction. The samples were characterized by means of x-ray powder diffraction at room temperature. The patterns were collected using the Bragg-Brentano θ-2θ geometry with a Rigaku D-Max system (rotating anode). The patterns were collected between 15° and 126° in steps of 0.03° and a counting rate of

4 s per step. Rietveld analysis was carried out using the FULLPROF package program.[8]

Magnetic measurements were made using a superconducting quantum interference device (SQUID) magnetometer from Quantum Design and a vibrating sample magnetometer (VSM) from AD Technologies.

X-ray absorption spectra were recorded at BM29 beamline of the ESRF in Grenoble (France).[9] The storage ring was operating at 6 GeV electron energy and ~200 mA electron current. The measurements were carried out in transmission mode on powder samples. The beam was monochromatized by a fixed-exit Si(111) double crystal at both the Cr *K* and the Re $L_{1,2,3}$ edges. Harmonic rejection better than 10^{-5} was achieved by using a Si mirror coating of the double flat mirror installed after the monochromator. The energy resolution, $\delta E/E$, was estimated to be about 7×10^{-5} and 1×10^{-4} at the Cr *K* and Re $L_{1,2,3}$ edges, respectively. XANES spectra were recorded at the Cr *K* and Re $L_{1,2,3}$ edges, whereas EXAFS spectra were taken at the Cr *K* and Re L_3 edges. The measurements were carried out at selected temperatures between 35 and 295 K. A Cr foil and a pellet of metallic Re were simultaneously measured for energy calibration at each respective absorption edge. The XANES spectra were normalized to the high energy part of each spectrum (~100 eV beyond the edge) after background subtraction. We have also recorded XANES spectra of Cr, Cr_2O_3, CrO_3, and $LaCrO_3$ as references for the Cr *K* edge. Re, ReO_2, ReO_3, and $Sr_{11}Re_4O_{24}$ were also measured as standards for the Re *L* edges.

The EXAFS structural analysis was performed using the ARTEMIS program,[10] which makes use of theoretical standards from FEFF6.[11] The fits were carried out in *R* space using a sine window and clusters of ~4 Å, which include contributions from the first, second, and third shells. Nevertheless, the discussion will be focused on the first coordination shell because it is correlated with the main physical properties.

III. RESULTS AND DISCUSSION

Sr_2CrReO_6 can be prepared as a single phase although some batches showed traces of metallic Re and $Sr_{11}Re_4O_{24}$. Sr_2CrReO_6 is cubic with an ordered arrangement of CrO_6 and ReO_6 octahedra with antisite defects as reported elsewhere.[7] The x-ray patterns of $Sr_{2-x}Ln_xCrReO_6$ always were composed of a main cubic phase contaminated with $Sr_{11}Re_4O_{24}$, as can be seen in Fig. 1. The ratio of the secondary phase tends to increase while the doping level increases. In this case, single-phase samples could only be obtained with Cr/Re > 1, suggesting an excess of Cr occupying Re sites. For instance, the x-ray patterns of $Sr_{1.5}La_{0.5}CrReO_6$ and $Sr_{1.5}La_{0.5}Cr_{1.125}Re_{0.75}O_6$ are compared in Fig. 1. The latter is single phase, and the only difference between both patterns concerns the presence of a secondary phase in the $Sr_{1.5}La_{0.5}CrReO_6$ sample. For all single-phase compounds, chemical analysis confirmed that the Cr/Re ratio is close to $(1+x/2)/(1-x/2)$, *x* being the rare-earth content. Moreover, the $Sr_{2-x}Ln_xCr_{1+x/2}Re_{1-x/2}O_6$ samples seem to be the only magnetic phase above room temperature because $Sr_{11}Re_4O_{24}$ only shows weak ferromagnetism below 10 K.[12] This feature

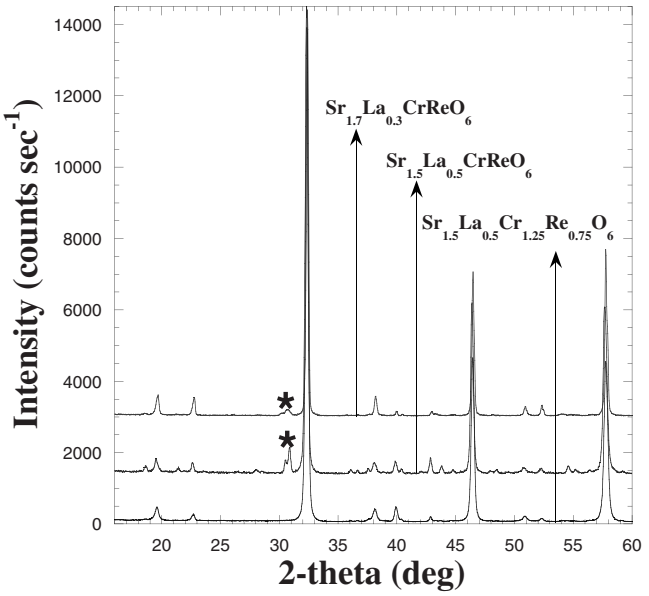

FIG. 1. From top to bottom, details of the x-ray patterns for $Sr_{1.7}La_{0.3}CrReO_6$, $Sr_{1.5}La_{0.5}CrReO_6$, and $Sr_{1.5}La_{0.5}Cr_{1.25}Re_{0.75}O_6$. Asterisk denotes the main peak for the $Sr_{11}Re_4O_{24}$ phase.

is clearly seen in Fig. 2, where magnetization curves for selected samples are plotted. The data were collected at 1 kOe on warming. Sr_2CrReO_6 orders ferromagnetically around 600 K, in agreement with previous studies.[2] The La addition leads to a decrease of magnetic moment, but the T_C remains almost constant, and this is true for both sets of samples, $Sr_{2-x}La_xCr_{1+x/2}Re_{1-x/2}O_6$ and $Sr_{2-x}La_xCrReO_6$.

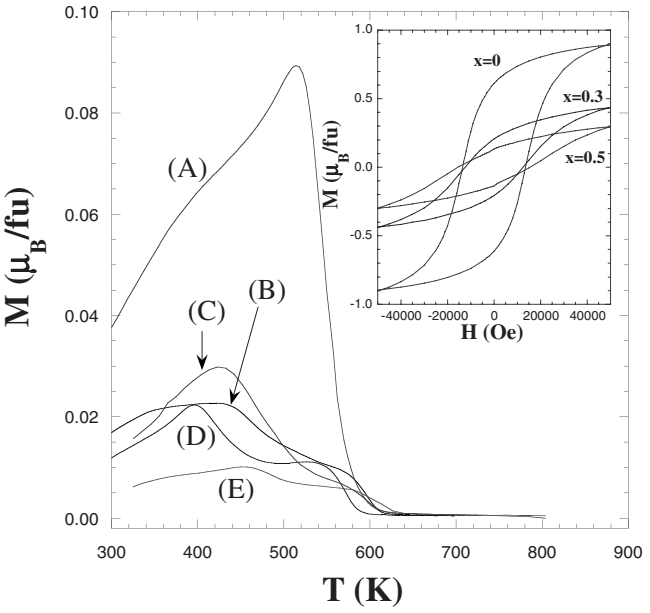

FIG. 2. Magnetization vs temperature curves for (A) Sr_2CrReO_6, (B) $Sr_{1.7}La_{0.3}Cr_{1.15}Re_{0.85}O_6$, (C) $Sr_{1.7}La_{0.3}CrReO_6$, (D) $Sr_{1.5}La_{0.5}Cr_{1.25}Re_{0.75}O_6$, and (E) $Sr_{1.5}La_{0.5}CrReO_6$, measured using a VSM setup and an external field of 1 kOe. Inset: Hysteresis loops of $Sr_{2-x}La_xCr_{1+x/2}Re_{1-x/2}O_6$ (x=0, 0.3, and 0.5) measured with a SQUID at 5 K.

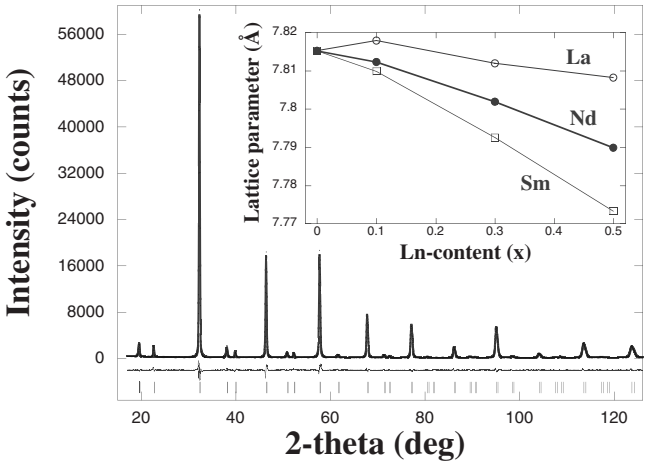

FIG. 3. Experimental (points), calculated (line), and difference x-ray patterns for $Sr_{1.7}La_{0.3}Cr_{1.15}Re_{0.85}O_6$. Allowed reflections are also indicated as bars at the bottom. Inset: Lattice parameter vs chemical composition for $Sr_{2-x}La_xCr_{1+x/2}Re_{1-x/2}O_6$ samples. Ln is given for each curve.

The differences observed below T_C may be ascribed to subtle changes in the magnetic anisotropy and the lack of magnetic saturation with an external field of 1 kOe. This fact is displayed in the magnetic isotherms measured at 5 K (see inset of Fig. 2). Magnetic saturation is not achieved at 5 T, and the magnetization at high field decreases with increasing La content. The hysteresis loops exhibit very large coercive fields (more than 1 T in some cases). We conclude that the $Sr_{2-x}Ln_xCr_{1+x/2}Re_{1-x/2}O_6$ phase is responsible for the magnetic behavior. Therefore, we will focus this work on the structural properties of $Sr_{2-x}Ln_xCr_{1+x/2}Re_{1-x/2}O_6$ single phases.

A. Crystal structure at room temperature

The room temperature x-ray patterns were used to determine the crystal structure of $Sr_{2-x}Ln_xCr_{1+x/2}Re_{1-x/2}O_6$, with $x=0$, 0.1, 0.3, and 0.5. All of the samples were refined as double perovskites in the cubic space group *Fm*-3*m* with a unit cell of $2a_p \times 2a_p \times 2a_p$, where a_p is the unit cell of the simple cubic perovskite. For instance, the refinement for $Sr_{1.7}La_{0.3}Cr_{1.15}Re_{0.85}O_6$ is shown in Fig. 3 and the refined parameters for the different samples are listed in Table I. The small number of peaks observed in the patterns indicates high crystal symmetry. Nevertheless, some features of the spectra have to be mentioned. First of all, the diffraction peaks are very broad, especially at high angles and for high Ln content. This fact can be indicative of a low crystallinity of the samples. Moreover, the refined temperature factors for oxygen atoms are very high and they increase as the Ln content increases (see Table I and compare with the values for the parent compound Sr_2CrReO_6). This could suggest the presence of oxygen vacancies, which would imply an oxidation of the Cr/Re atoms. Another possibility could be a structural microstrain induced by either antisite defects or Sr/Ln disorder. In any case, the cubic cell may be an average structure for a set of random distortions and the actual cell for these compounds would have a lower symmetry. Only the pattern of $Sr_{1.5}Sm_{0.5}Cr_{1.25}Re_{0.75}O_6$ exhibits very weak and broad superstructure peaks that can be indexed in a monoclinic structure with $P2_1/n$ symmetry and unit cell dimensions $\sqrt{2}a_p \times \sqrt{2}a_p \times 2a_p$. This space group is typical of DP showing a combination of tilting octahedra, in phase about [001] and out of phase about [110].[13] Our efforts to analyze the $Sr_{1.5}Sm_{0.5}Cr_{1.25}Re_{0.75}O_6$ pattern in the $P2_1/n$ space group always led to unstable refinements, probably due to the aforementioned effects. Therefore, we only report the refinement in the cubic group for the sake of comparison with the rest of the series.

The cell size decreases following the trend of the lanthanide contraction that overcomes other contributions (see inset of Fig. 3). For the sake of comparison, an effective electron doping was reported to produce volume expansion in Mo-based double perovskites.[3] The space group *Fm*-3*m* allows an ordered 1:1 arrangement of the Cr and Re atoms over the two possible sites, 4*a* at (0, 0, 0) and 4*b* at $(\frac{1}{2},0,0)$.

TABLE I. Refined structural parameters (lattice, temperature factor, atomic occupation, and fractional coordinate) and reliability factors (as defined in Ref. 8) for Sr_2CrReO_6 and $Sr_{2-x}Ln_xCr_{1+x/2}Re_{1-x/2}O_6$. Ln_x is given for each column.

	Sr_2CrReO_6	$La_{0.1}$	$La_{0.3}$	$La_{0.5}$	$Nd_{0.1}$	$Nd_{0.3}$	$Nd_{0.5}$	$Sm_{0.1}$	$Sm_{0.3}$	$Sm_{0.5}$
a (Å)	7.8152(1)	7.8179(1)	7.8120(1)	7.8082(1)	7.8123(1)	7.8019(1)	7.7899(1)	7.8098(1)	7.7926(1)	7.7733(1)
Sr at $(\frac{1}{2}\ \frac{1}{2}\ \frac{1}{2})$										
B (Å^2)	0.86(2)	0.85(2)	1.20(2)	1.01(2)	0.89(2)	0.82(2)	1.39(2)	0.97(1)	1.11(2)	1.17(4)
Cr at (0 0 0)										
B (Å^2)	0.39(3)	0.22(4)	0.24(4)	0.32(5)	0.45(5)	0.16(9)	0.39(6)	0.27(3)	0.21(4)	0.16(5)
Occ. Cr/Re	86/14	85/15	86/14	87/13	83/17	84/16	85/15	88/12	81/19	82/18
Re at $(\frac{1}{2}\ 0\ 0)$										
B (Å^2)	0.06(3)	0.08(2)	0.20(2)	0.14(3)	0.29(3)	0.08(3)	0.42(3)	0.21(2)	0.28(3)	0.34(5)
Occ. Cr/Re	14/86	20/80	29/71	38/62	22/78	31/69	40/60	17/83	34/66	43/57
O at (*x* 0 0)										
x	0.2505(4)	0.2505(5)	0.2507(5)	0.2503(6)	0.2509(7)	0.2506(5)	0.2507(6)	0.2506(4)	0.2504(6)	0.2503(6)
B (Å^2)	0.74(5)	0.90(7)	1.24(4)	0.88(8)	1.03(11)	1.23(6)	1.34(9)	1.11(6)	1.77(7)	2.29(9)
R_{wp}/R_{Bragg}	7.9/4.2	9.9/3.7	9.1/3.2	8.6/4.1	10.3/3.9	8.5/4.7	9.1/3.4	7.6/4.2	8.2/3.4	11.5/4.5

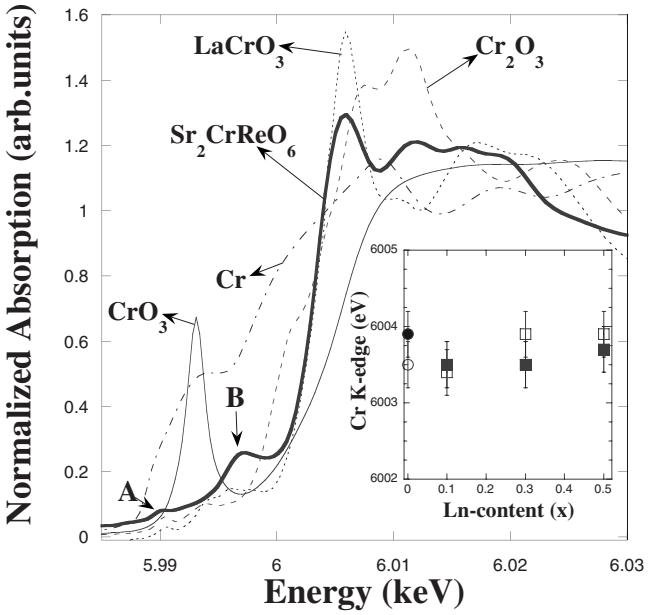

FIG. 4. Normalized Cr *K*-edge XANES spectra for metallic Cr (dot-dashed line), Cr_2O_3 (dashed line), $LaCrO_3$ (dotted line), Sr_2CrReO_6 (thick line), and CrO_3 (thin line). *A* and *B* denote preedge features at the Sr_2CrReO_6 spectrum. Inset: Edge position, defined as the maximum of the first derivative of the normalized XANES, for $Sr_{2-x}Nd_xCr_{1+x/2}Re_{1-x/2}O_6$ (filled squares) and $Sr_{2-x}Sm_xCr_{1+x/2}Re_{1-x/2}O_6$ (open squares) at 295 K. The filled and open symbols for $x=0$ correspond to the values at 35 and 295 K, respectively.

The site occupation was refined under the constraint that the total occupation (addition of both sites) was equal to the nominal stoichiometry. The results indicate that the parent compound contains antisite defects (around 15%) as reported elsewhere.[7] Here, 0% means a full ordering, while 50% implies complete disorder. The addition of the lanthanide and, accordingly, the excess of Cr imply an increase of the Cr occupation at the 4*b* site (or "Re site"), whereas an almost constant mixture of Cr and Re remains on the 4*a* site. If this trend was followed in the whole $Sr_{2-x}Ln_xCr_{1+x/2}Re_{1-x/2}O_6$ series, one would expect that superstructure peaks arising from a DP structure would exist up to $x\sim 1.4$. Above this value, a solid solution of both metals would be expected, giving rise to a single perovskite unit cell.

B. Cr *K*-edge x-ray absorption near edge structure

The aforesaid limitation of the diffraction study indicates the need for a spectroscopic investigation to fully characterize this system. X-ray absorption spectroscopy probes local structure around the photoabsorbing atom and allows us to determine if the charge distribution between Cr and Re atoms is modified after lanthanide addition. Such a change in the charge distribution was observed in Mo-based DP depending on the alkaline-earth atom.[14]

Figure 4 shows the Cr *K*-edge XANES spectra of Sr_2CrReO_6, the Cr^{3+} standards $LaCrO_3$ and Cr_2O_3, the Cr^{6+} standard CrO_3, and metallic Cr. This edge is highly sensitive to the local structure and, for instance, CrO_3 exhibits a sharp peak in the preedge region at 5993 eV, which is ascribed to the dipole-forbidden transition $1s\rightarrow 3d$. The presence of this strong feature is in agreement with a tetrahedral coordination for the Cr^{6+} without an inversion center.[15] The rest of the Cr oxides with an octahedral coordination show less intense preedge features. The absorption edge position is related to the Cr oxidation state, as can be seen in Fig. 4. The absorption edge shifts to higher energy with increasing Cr valence. The rising part of the Sr_2CrReO_6 main edge coincides with that of the $LaCrO_3$. According to the fact that both compounds have a similar crystal structure (perovskite), a formal Cr^{3+} oxidation state is deduced for Sr_2CrReO_6. The other Cr^{3+} standard, Cr_2O_3, also exhibits a similar chemical shift although, in this case, the edge shows a bimodal feature that may be ascribed to the different crystal structure (rutile). The spectra for the rest of the $Sr_{2-x}Ln_xCr_{1+x/2}Re_{1-x/2}O_6$ samples (Ln=Nd or Sm) are identical to that of Sr_2CrReO_6. We have taken the strong maximum at the first derivative of the absorption spectra as the position for the absorption edge. Obtained data are plotted in the inset of Fig. 4 for the two series. We have also included the data for the parent compound at two temperatures. It is clear that the edge position remains almost constant within the experimental error. Therefore, there is no significant change in the oxidation state of Cr atoms after replacing Sr by rare earths and it remains Cr^{3+} for all the studied samples.

The main difference between $LaCrO_3$ and the DP concerns the preedge region. Both kinds of compounds present a small peak at around 5990 eV, denoted as *A* in Fig. 4. However, the DP shows a prominent feature at ~5997 eV, denoted as *B*, which is completely different from the features observed in $LaCrO_3$. There are two possibilities to account for *B*. Compounds containing Cr^{2+} species display a similar feature at the same energy.[16] However, there is a significant chemical shift (~4 eV) between Cr^{2+} and Cr^{3+} as can be seen in the XANES spectra reported for compounds with Cr^{2+}.[16,17] Taking into account the absence of chemical shift between our DP and $LaCrO_3$, we can infer the presence of only Cr^{3+} in these compounds. A similar oxidation state was found for Cr atoms in the XANES of Mo-based DP.[14,18]

Preedge features at transition-metal *K* edges are mainly attributed to quadrupole $1s\rightarrow 3d$ transitions since this transition is dipole forbidden. Quadrupole transitions are orders of magnitude weaker than dipole transitions,[19] and the increase in the intensity of the preedge features was attributed in some cases to the spreading of 4*p* band, which mixes into 3*d* orbitals.[20–22] Another possibility is that feature *B* can be related to the Cr 3*d*-O 2*p* hybridization since theoretical studies on binary oxides have demonstrated that transitions to hybridized 3*d*-like orbitals made up of 3*d* metal orbitals and 2*p* oxygen orbitals can account for the presence of significant dipole transitions.[23] Both mechanisms provide some electric dipole allowed $1s\rightarrow np$ character to the transition and adds intensity to the preedge features. In these DP, the transition metal is surrounded by six oxygens, forming an octahedron (as occurs in compounds studied in Ref. 23), and neighboring octahedra strongly interact with each other, producing extended energy bands.

In order to accurately compare the intensities of the preedge peaks, we have fitted the normalized spectra of Fig.

4 with the addition of a symmetric Lorentzian and a hyperbolic tangent (tanh) function between 5.97 and 6.01 keV. Selecting the white line maximum and the inflection point as starting values for the centers of the Lorentzian and tanh parts, convergence is easily achieved. In fact, there is no need to remove the preedge range (between 5.97 and 6.02 keV) from the fit range because the same result is obtained in both conditions. Figure 5(a) depicts the absorption edge and the fit for Sr_2CrReO_6 at 295 K. The inset of Fig. 5(a) shows the result of subtracting the base line (fit) from the experimental spectra. Three features are clearly observed in the preedge region. In addition to the *A* and *B* peaks, a shoulder (denoted as *C* in the inset) is clearly noticeable. The preedge peaks could not be fitted to Lorentzian functions satisfactorily, but accurate fits were obtained by using Gaussian functions as shown in the same inset. This fit reveals that the *B*-peak area is 1 order of magnitude higher than any of the other two peaks and that the presence of dipolar contributions are more likely for the *B* peak.

The preedge features of $Sr_{2-x}Nd_xCr_{1+x/2}Re_{1-x/2}O_6$ samples are compared to those of $LaCrO_3$ in Fig. 5(b). The small peak *A* is present for all samples at the same energy and with similar intensity. This peak is ascribed to pure quadrupole transitions as occur in related oxides,[23,24] and it is extremely sensitive to the 3*d* orbital occupation as demonstrated for TiO_2.[23] In this way, it further supports the presence of Cr^{3+} in DP. The rest of the preedge features in DP are completely different from $LaCrO_3$. Sr_2CrReO_6 has the strongest peak *B*, whose intensity decreases with increasing content of the rare earth. In the inset of Fig. 5(b) is plotted the area of this peak for the DP studied, showing a clear decrease as the rare-earth content is increased. A decrease in the electrical conductivity of these samples with increasing Ln concentration has been reported previously.[4] This result agrees with a concomitant decrease of the orbital overlapping between Cr and oxygen atoms so that we can assume that the intensity of *B* would be related to the degree of Cr-O covalency.

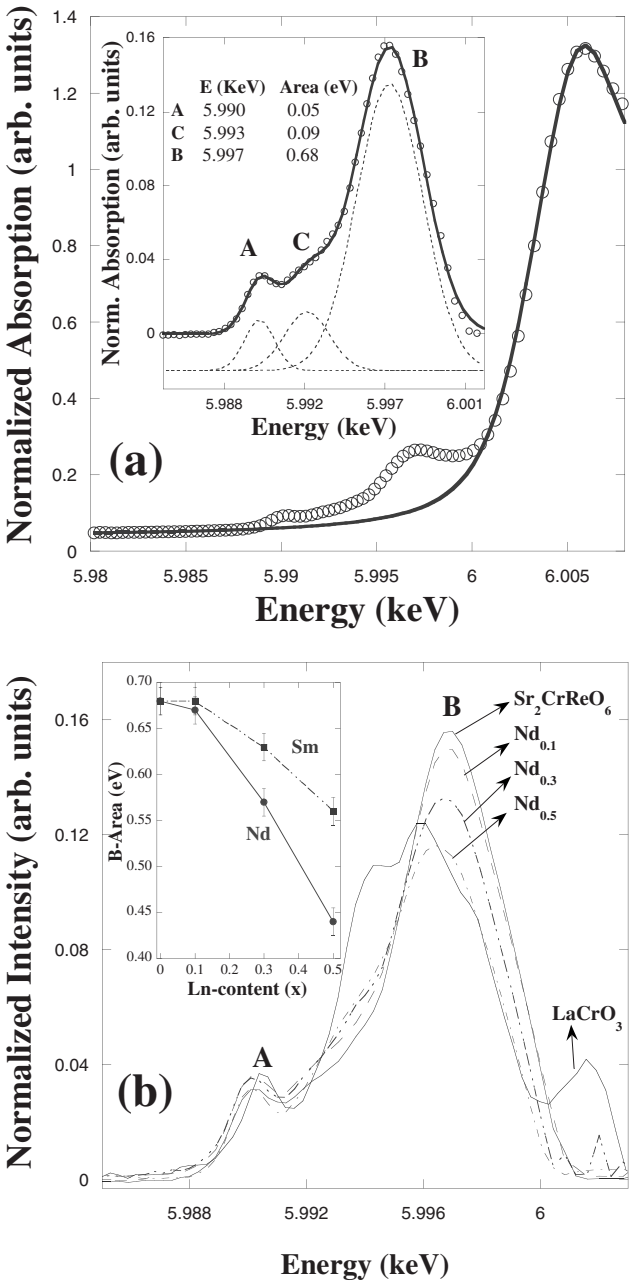

FIG. 5. (a) Normalized Cr *K*-edge spectrum (circles) for Sr_2CrReO_6 at 290 K together with the base line obtained from the fit to a tanh and a Lorentzian function (continuous line). Inset: Preedge features (circles) from the normalized spectrum after the subtraction of the base line. The features have been fitted to three Gaussian functions (continuous line) whose position and areas are also indicated. The Gaussian peaks are shifted downwards (dotted lines) for the sake of clarity. (b) Detail of the preedge structures in the normalized XANES spectra after background subtraction for $Sr_{2-x}Nd_xCr_{1+x/2}Re_{1-x/2}O_6$ ($x \leqslant 0.5$) and $LaCrO_3$. Inset: Value of the *B* area for $Sr_{2-x}Nd_xCr_{1+x/2}Re_{1-x/2}O_6$ and $Sr_{2-x}Sm_xCr_{1+x/2}Re_{1-x/2}O_6$ series.

C. Re *L*-edge x-ray absorption near edge structure

Figure 6 shows the Re L_1-edge XANES spectra of Sr_2CrReO_6, the Re^{4+} standard ReO_2, the Re^{6+} standard ReO_3, the $Re^{6.5+}$ standard $Sr_{11}Re_4O_{24}$, and metallic Re. This edge is caused by $2s \rightarrow 6p$ transitions and it provides similar information as a *K* edge.

ReO_3 shows a crystal cell similar to a DP, but with vacancies at the Sr position. $Sr_{11}Re_4O_{24}$ is a Sr-deficient DP with Re in two oxidation states, half in 6+ and half in 7+ (average 6.5+).[12] In both cases, there are ReO_6 octahedra sharing corners. ReO_2 is also formed by ReO_6 octahedra but, in this case, they share edges.[25] It is clear that the edge position for Sr_2CrReO_6 lies between Re^{4+} and Re^{6+} standards, as can be seen in Fig. 6. The rest of DP in our study (not shown here) showed an L_1-edge spectrum nearly identical to that of Sr_2CrReO_6. The first derivative of the Re L_1-edge XANES spectra, shown in the inset of Fig. 6, reveals a bimodal feature for the edge region. The higher energy derivative peak is quite sensitive to the chemical shift as can be seen in this inset. From this plot, we realized that there is a linear relationship between the energy position of this peak and the nominal 5*d*-orbital occupation of the standards, which is plotted in Fig. 7. We have taken this derivative peak centroid as absorption edge for all samples and its value is close to

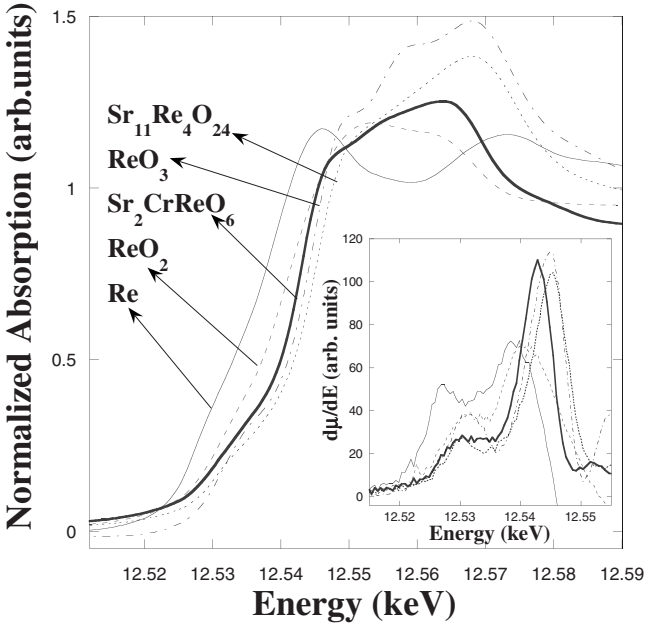

FIG. 6. Normalized Re L_1-edge XANES spectra for selected samples. Inset: First derivative of these spectra around the absorption edge.

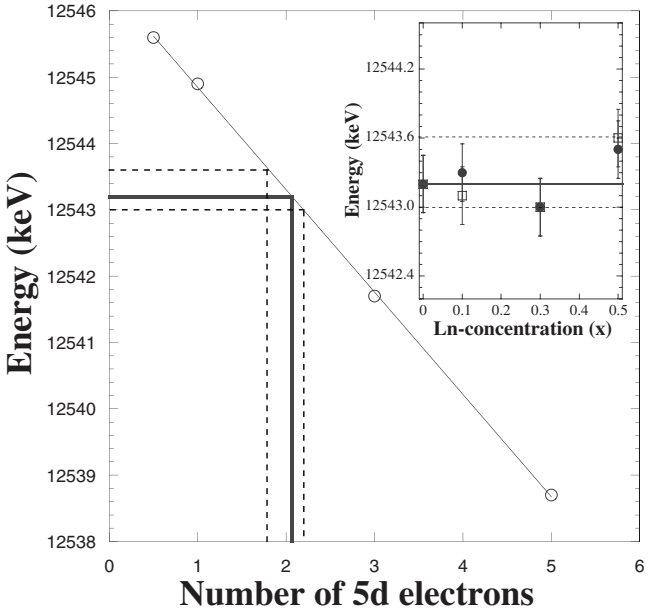

FIG. 7. Re L_1-edge position vs $5d$ electron occupation for Re standards (circles). A linear fit is also displayed. The thick line relates the edge position for Sr_2CrReO_6 to the $5d$ occupation. Dashed lines limit the region for the edge position of $Sr_{2-x}Nd_xCr_{1+x/2}Re_{1-x/2}O_6$ and $Sr_{2-x}Sm_xCr_{1+x/2}Re_{1-x/2}O_6$ samples. Inset: Re L_1-edge position for $Sr_{2-x}Nd_xCr_{1+x/2}Re_{1-x/2}O_6$ (circles) and $Sr_{2-x}Sm_xCr_{1+x/2}Re_{1-x/2}O_6$ (squares) series. The lines have the same meaning as the main figure.

the half-height of the absorption edge. The position for the undoped sample is in agreement with an electronic configuration close to $5d^2$, which is the expected electronic configuration of a Re^{5+} ion. The edge position for the rest of the Ln-based DP is displayed in the inset of Fig. 7. There is no clear trend for any edge position shift with the Ln concentration and, in fact, the edge position seems to remain constant within the experimental error. The inferred electronic configuration for $Sr_{2-x}Ln_xCr_{1+x/2}Re_{1-x/2}O_6$ samples always lies close to the value expected for Re^{5+}, i.e., within the dashed lines plotted in Fig. 7. Consequently, the Re L_1-edge XANES spectra agree with a formal Re^{5+} valence for all Ln-based DP.

Figure 8 shows the Re L_2-edge and Re L_3-edge XANES spectra for selected DP and reference compounds. The spectra of DP are characterized by strong white lines as expected from the presence of empty $5d$ states.[26] The absorption at the Re L_2 or Re L_3 edges is caused by the ionization of a $2p_{1/2}$ or $2p_{3/2}$ core electron, respectively. Therefore, these edges probe the $2p_{1/2} \rightarrow 5d_{3/2}$ (L_2 edge) and $2p_{3/2} \rightarrow 5d_{3/2}, 5d_{5/2}$ (L_3 edge) transitions. None of these edges seems to be very sensitive to the chemical shift and, for instance, the edge position of $Sr_{11}Re_4O_{24}$ and ReO_3 is very similar at the L_2 edge, whereas the L_3 edge of $Sr_{11}Re_4O_{24}$ is at a lower energy in spite of its higher Re valence. For DP and ReO_2, both L_2 and L_3 edges lie at similar energy positions.

The reference compounds, metallic Re and ReO_2, have a broad peak at both edges. The rest of the samples present a double peak in each edge. The presence of a double peak is usually found in $L_{2,3}$ edges of transition metals with an octahedral coordination, and it is generally ascribed to the crystal field splitting of d orbitals into t_{2g} and e_g states.[27] In the case of Re L_2 edge, the stronger peak occurs at lower energies, while the opposite is observed for the Re L_3 edge as found in Fe-based DP.[28]

We have fitted both absorption edges to two symmetric Lorentzian functions and a tanh. Figure 9(a) depicts the fit of L_2 edge for Sr_2CrReO_6 in the range between 11.94 and 11.98 keV. Normally, the intensity of the white lines in the $L_{2,3}$ edges can be correlated to the number of d holes, allowing an estimation of the oxidation state. A first sight to the standard compounds in Fig. 8 reveals that different trends are followed for L_2 or L_3 edges. These differences may be ascribed to different effects such as the extent to which the $5d$ electrons are part of a conduction band which tends to delocalize the final state, the $5d$ spin-orbit coupling, and multiplet effects, i.e., correlation effects between the $2p$ core hole and the $5d$ holes.[29] It was reported that L_2 edges are less affected by multiplet effects than L_3 edges for $4d$ systems,[30] and this also seems to work for our $5d$ system. We have calculated the areas of the white lines for all compounds including the standards, as indicated in Fig. 9(a). The areas were approximated to FWHM $\times$ height, FWHM being the full width at half maximum. There is no clear relationship between the white line area and the $5d$ occupation in the case of the L_3 edge. However, there is a linear relationship for the case of the L_2 edge, as can be seen in Fig. 9(b). The total area (P_1+P_2) for our DP samples ranges between 18.9 and 19.6 eV [see inset of Fig. 9(b)], which agrees with an electronic configuration close to $5d^2$. This assignment concurs with the previous result obtained in the analysis of the L_1 edge.

D. Extended x-ray absorption five structure

The Cr K-edge EXAFS spectra were collected for the $Sr_{2-x}Sm_xCr_{1+x/2}Re_{1-x/2}O_6$ samples up to $k \sim 13$ Å^{-1}. These

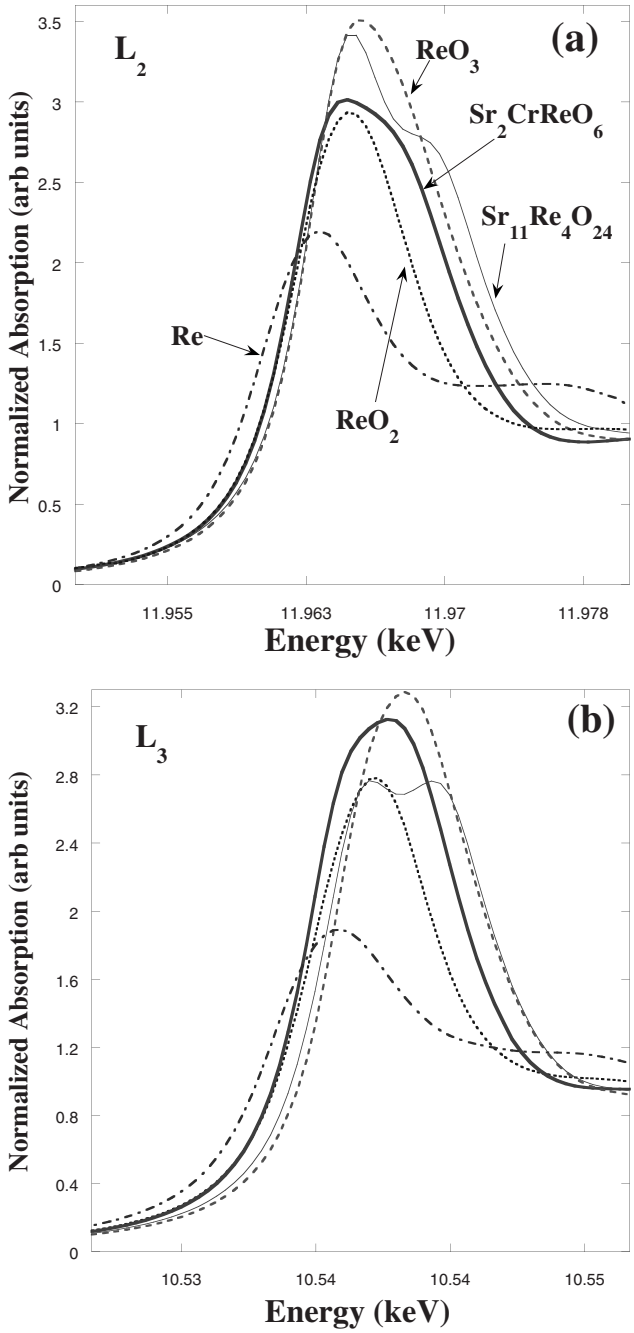

FIG. 8. Normalized (a) Re L_2-edge and (b) Re L_3-edge XANES spectra of Sr_2CrReO_6 and selected references.

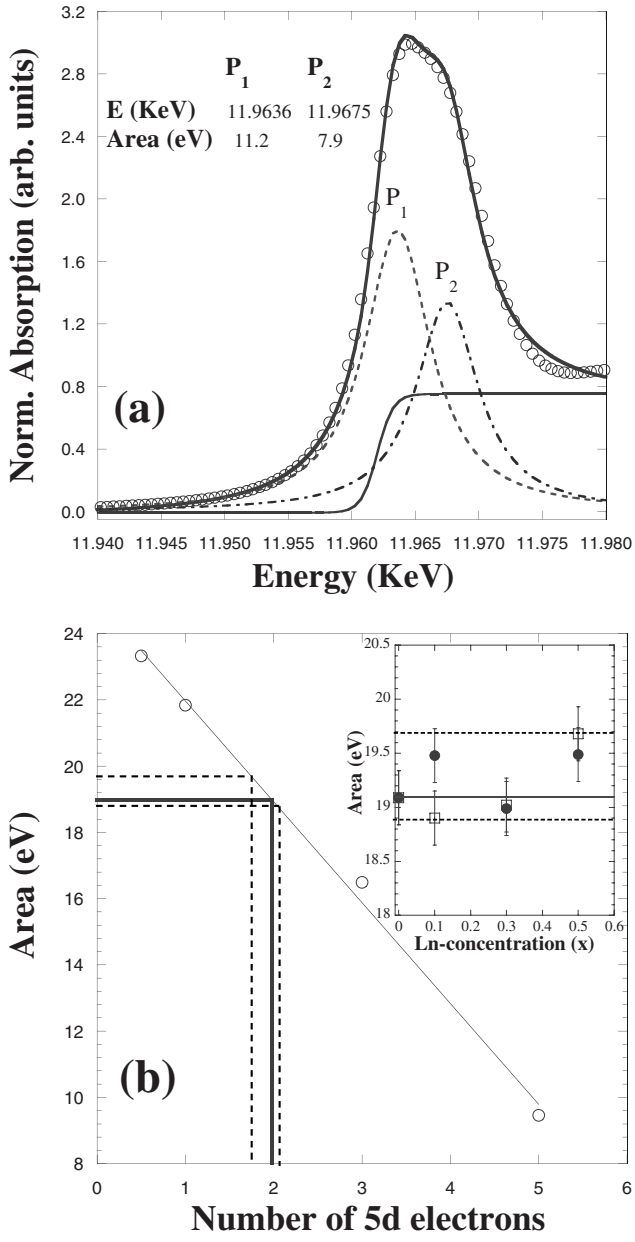

FIG. 9. (a) Normalized Re L_3-edge spectrum for Sr_2CrReO_6 at 290 K (circles) and the fit (continuous line) using the addition of two Lorentzian functions and one tanh function. These functions are also depicted below the fit. The position and area for both peaks are also indicated. (b) Area of the total L_2 white line vs $5d$ electron occupation for Re standards (circles). A linear fit is also displayed. The thick line relates the area for Sr_2CrReO_6 to the $5d$ occupation. Dashed lines limit the region for calculated areas of $Sr_{2-x}Nd_xCr_{1+x/2}Re_{1-x/2}O_6$ and $Sr_{2-x}Sm_xCr_{1+x/2}Re_{1-x/2}O_6$ samples. Inset: Values of the areas for $Sr_{2-x}Nd_xCr_{1+x/2}Re_{1-x/2}O_6$ (circles) and $Sr_{2-x}Sm_xCr_{1+x/2}Re_{1-x/2}O_6$ (squares) compounds vs the Ln content (x). The lines have the same meaning as the main figure.

measurements were not possible for the Nd-based compounds due to the proximity of the Nd L_3 and Cr K edges. The Fourier transform (FT) of the k-weighted EXAFS spectra was calculated between 3 and 12 $Å^{-1}$ using a sine window, and the structural features up to 6 Å are shown in Fig. 10(a). The FT shows a strong peak at ~1.55 Å, corresponding to the Cr-O distance without a phase-shift correction. The second and third coordination shells show two peaks between 2.5 and 3.8 Å. Contributions from single, Cr-Re and Cr-Sr(Sm), paths, together with multiple-scattering paths, mainly Cr-O-O and Cr-O-Re, account for both peaks. The structural analysis between 1 and 4 Å was performed using the ARTEMIS software[10] in the R-space fitting mode. The fits are displayed in Fig. 10(a), and the main structural parameters for the first shell are summarized in Table II for two selected temperatures. In these fits, the coordination numbers were fixed to their crystallographic values and the amplitude

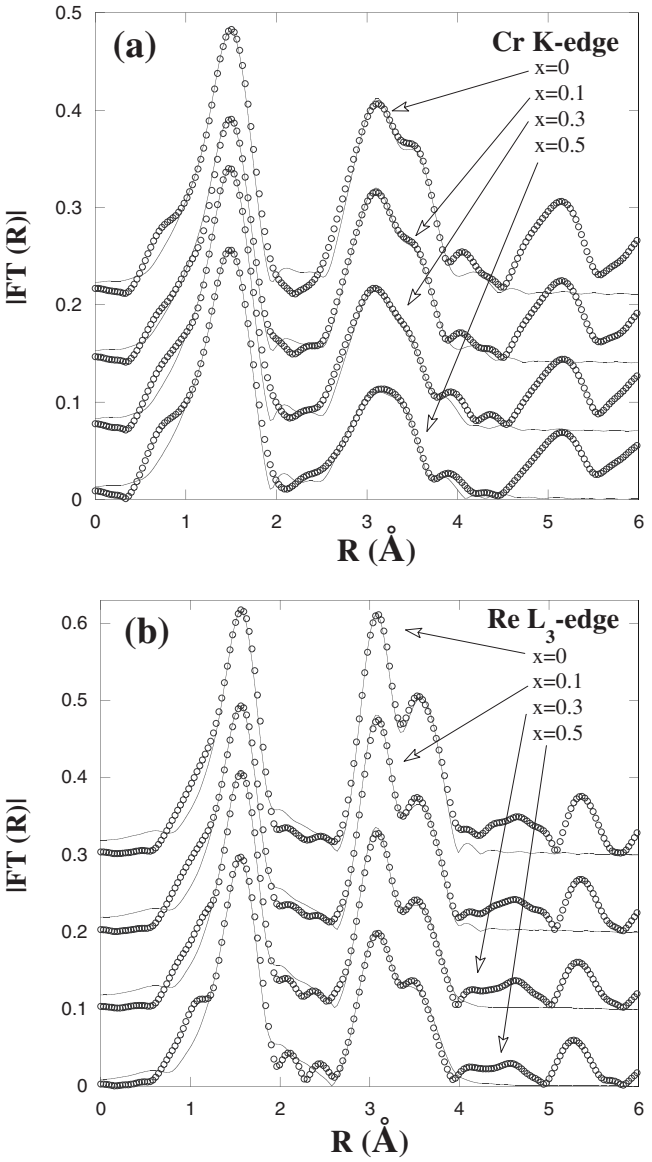

FIG. 10. (a) Fourier transforms of the $k\chi(k)$ EXAFS spectra at the Cr K edge for $Sr_{2-x}Sm_xCrReO_6$ series at 35 K. Solid lines are the best-fit simulations only considering contributions between 1 and 4 Å. (b) Fourier transforms of the $k\chi(k)$ EXAFS spectra at the Re L_3 edge for $Sr_{2-x}Sm_xCrReO_6$ series at 35 K. Solid lines are the best-fit simulations only considering contributions between 1.2 and 3.9 Å. The x values are given for each curve and the spectra are shifted upwards for the sake of clarity.

reduction factor s_0^2 was set at 0.7, in agreement with previous calculations.[31] Therefore, only bond lengths, Debye-Waller factors, and threshold energy (E_0) were refined. The interatomic distances remain practically constant in the whole series and minor changes are noticed with decreasing temperature. All samples exhibit an average Cr-O bond length close to 1.955 Å, similar to either the reported value[32] in $LaCrO_3$ or the theoretical value expected for a Cr^{3+} ion.[33] Therefore, the EXAFS analysis concurs with the XANES study that Ln addition does not induce significant changes in the Cr oxidation state.

EXAFS spectra were also measured at the Re L_3 edge. In this case, measurements of the $Sr_{2-x}Nd_xCr_{1+x/2}Re_{1-x/2}O_6$ samples were also possible, with identical results to the Sm-based compounds. Oscillations at this edge are still visible up to 15 $Å^{-1}$, and the FT of the k-weighted spectra shown in Fig. 10(b) was calculated between 2.8 and 15 $Å^{-1}$ using a sine window. The FT spectra reveal similar features with a strong peak around 1.5 Å (without a phase-shift correction), which corresponds to the Re-O distance. Also two noticeable peaks are observed between 2.5 and 3.8 Å, ascribed to Re-Cr, Re-Sr(Sm) single-scattering paths and multiple-scattering contributions. Fits in R space were carried out between 1.2 and 3.9 Å, as can be seen in Fig. 10(b). In this case, the s_0^2 factor was fixed[31] to 0.78 and the crystallographic values were taken as coordination number. Only the E_0, bond lengths, and Debye-Waller factors were refined as in the Cr K edge case. The structural parameters are also summarized in Table II. The Re-O bond lengths also concur with the previous crystallographic study and their values are around 1.935 Å, very similar to those found in other double perovskites showing Re^{5+}.[28] Moreover, oxides with formal Re^{6+}, such as ReO_3, show Re-O distances[34] around 1.87 Å, significantly smaller than the present case. Therefore, the EXAFS analysis agrees with the presence of Re^{5+} for all samples.

The data from Table II also reveal that CrO_6 octahedron is a bit bigger than the ReO_6 one. However, the great similitude between Re-O and Cr-O distances explains the tendency to form antisite defects in these compounds. Both atoms have very symmetric octahedral environments as deduced from the small value of the Debye-Waller factors found. These factors remain small even for samples with high Ln content, where more Cr is located on the Re site with slightly different distances. This suggests that our EXAFS analysis is not sensitive to this minor local change. In fact, the environment changes produced by antisite defects in these materials are still lower than the spread of Cr-O distances (between 1.94 and 1.99 Å) in the reference compound $LaCrO_3$.[32]

IV. CONCLUSIONS

In the present study, we have shown that the synthesis of $Sr_{2-x}Ln_xCrReO_6$ single phases is not possible using conventional synthetic routes. Competitive $Sr_{2-x}Ln_xCr_{1+x/2}Re_{1-x/2}O_6$ and $Sr_{11}Re_4O_{24}$ phases are formed. This implies the significant difficulty in preparing electron doped DP in these Cr-based systems. Magnetic measurements confirm that $Sr_{2-x}Ln_xCr_{1+x/2}Re_{1-x/2}O_6$ compounds are the only magnetic phases above room temperature. They exhibit large coercive fields, and the magnetic moment decreases following the trend of the Cr occupation in the Re site, in agreement with a ferromagnetic coupling between both sublattices. However, the parent compound shows a magnetic moment higher than that expected from the spin-only contribution, suggesting an important role from unquenched angular contribution.[7]

Then, we have characterized the structural properties of a different family of DP, the $Sr_{2-x}Ln_xCr_{1+x/2}Re_{1-x/2}O_6$ series, with Ln=La, Nd, or Sm. The x-ray patterns of these compounds can be indexed using a cubic face-centered cell. The Rietveld refinement confirms this fact although it suggests

TABLE II. Structural parameters for the first coordination shell (bond lengths and Debye-Waller factors). They are extracted from the fits of Fig. 10 for Sr_2CrReO_6 (denoted as Sr_2) and $Sr_{2-x}Ln_xCr_{1+x/2}Re_{1-x/2}O_6$ (denoted as Ln_x) samples. The reliability factors, defined in Refs. 10 and 11, refer to the whole fit (not only the first shell). Coordination number is fixed to 6 for all cases.

		Cr K edge			Re L_3 edge		
Sample	T (K)	Cr-O (Å)	$\sigma^2 \times 10^{-3}$ (Å^2)	R_F	Re-O (Å)	$\sigma^2 \times 10^{-3}$ (Å^2)	R_F
Sr_2	25	1.954(12)	1.5(7)	0.012	1.935(4)	1.3(5)	0.016
	290	1.957(12)	1.8(7)	0.015	1.937(5)	1.7(5)	0.014
$Sm_{0.1}$	25	1.947(12)	2.0(7)	0.015	1.933(4)	1.8(5)	0.013
	290	1.951(12)	2.2(7)	0.015	1.935(5)	2.1(4)	0.014
$Sm_{0.3}$	25	1.954(12)	1.5(7)	0.017	1.935(4)	1.6(5)	0.018
	290	1.960(12)	1.9(7)	0.018	1.936(5)	2.0(5)	0.017
$Sm_{0.5}$	25	1.961(12)	2.2(7)	0.014	1.935(5)	1.5(4)	0.019
	290	1.965(12)	2.4(7)	0.019	1.937(4)	2.1(5)	0.017
$Nd_{0.1}$	25				1.933(5)	1.6(5)	0.014
	290				1.934(5)	1.7(4)	0.016
$Nd_{0.3}$	25				1.939(4)	1.2(6)	0.018
	290				1.940(5)	1.6(5)	0.02
$Nd_{0.5}$	25				1.937(4)	1.3(5)	0.019
	290				1.939(4)	2.4(6)	0.017

the presence of microstrain or defects for samples with a high Ln content. This may be ascribed to the smaller size of Ln^{3+}, especially in the case of Sm^{3+}. A consequence of this microstrain is the presence of large temperature factors for oxygen atoms, making the calculation of bond lengths less reliable. In order to complete this characterization, we have investigated the local structure of both Re and Cr in the $Sr_{2-x}Ln_xCr_{1+x/2}Re_{1-x/2}O_6$ DP. The sensitivity of the XANES technique has been used to check the oxidation state of both metals. In this way, the chemical shift of the Cr K edge revealed the presence of Cr^{3+} ions for all compounds. On the other hand, the edge position of the Re L_1 spectra agrees with the presence of Re^{5+} in the same compounds. Accordingly, we have tested the relationship between the area of the Re $L_{2,3}$ white lines and the unoccupied $5d$ electronic states. We have found a linear relationship at the L_2 edge, whereas the L_3 edge seems to be less appropriate for this goal due to multiplet effects, as reported previously for $4d$ systems.[30] The inferred $5d$ occupation also agrees with the presence of Re^{5+} for all compounds, in agreement with the Re L_1 edge results.

The EXAFS analysis gave Re–O and Cr–O bond lengths in agreement with the crystallography. Such distances do not vary with the doping ratio and concur with the expected values for Re^{5+} and Cr^{3+} oxides. Therefore, our spectroscopic study reveals the absence of change in the oxidation state of Cr and Re after the addition of Ln, i.e., the absence of electron doping as expected from the nominal stoichiometry.

The absence of electron doped phases in this system might be explained on the basis of the strong stability of the electronic Cr^{3+}-O-Re^{5+} configuration as inferred from our spectroscopic work. The replacement of only Sr^{2+} by La^{3+} implies the injection of an additional electron to the former sublattice. Neither Cr^{2+}-O-Re^{5+} nor Cr^{3+}-O-Re^{4+} seemed to be more stable than the mentioned configuration. Instead of doped samples, competitive $Sr_{2-x}Ln_xCr_{1+x/2}Re_{1-x/2}O_6$ phases are formed with a decrease in the Cr-O-Re coupling, owing to the increase of Cr-O-Cr paths. This coupling diminution is also correlated to a decrease in the Cr-O covalency observed in the attenuation of the B-peak intensity at the Cr K edge.

ACKNOWLEDGMENTS

The authors acknowledge financial support from CICyT (Project Nos. MAT2005-04562 and MAT2005-05565-C02-02) and DGA (CAMRADS and PIP018/2005). The authors thank ESRF for granting beam time and the BM29 team for help during the experiment. The authors also acknowledge P.A. Algarabel for the availability of magnetic measurements at high temperature with the VSM setup and R. Córdoba for help in sample preparation.

*Corresponding author; jbc@unizar.es

[1] K. L. Kobayashi, T. Kimura, H. Sawada, K. Terakura, and Y. Tokura, Nature (London) **395**, 677 (1998); D. Serrate, J. M. De Teresa, and M. R. Ibarra, J. Phys.: Condens. Matter **19**, 023201 (2007).

[2] J. Blasco, C. Ritter, L. Morellón, P. A. Algarabel, J. M. De Teresa, D. Serrate, J. García, and M. R. Ibarra, Solid State Sci. **4**, 651 (2002); H. Kato, T. Okuda, Y. Okimoto, Y. Tomioka, Y. Takenoya, A. Ohkubo, M. Kawasaki, and Y. Tokura, Appl. Phys. Lett. **81**, 328 (2002); G. Subias, J. Garcia, and J. Blasco, Phys. Rev. B **71**, 155103 (2005).

[3] J. Navarro, C. Frontera, Ll. Balcells, B. Martínez, and J. Fontcuberta, Phys. Rev. B **64**, 092411 (2001); D. Serrate, J. M. De Teresa, J. Blasco, M. R. Ibarra, L. Morellón, and C. Ritter, Appl. Phys. Lett. **80**, 4573 (2002); Eur. Phys. J. B **39**, 35 (2004).

[4] J. M. Michalik, J. M. De Teresa, D. Serrate, J. Blasco, and M. R. Ibarra, J. Magn. Magn. Mater. **316**, 413 (2007).

[5] Y. Krockenberger, K. Mogare, M. Reehuis, M. Tovar, M. Jansen, G. Vaitheeswaran, V. Kanchana, F. Bultmark, A. Delin, F. Wilhelm, A. Rogalev, A. Winkler, and L. Alff, Phys. Rev. B **75**, 020404(R) (2007).

[6] M. C. Sánchez, J. García, J. Blasco, G. Subías, and J. Pérez-Cacho, Phys. Rev. B **65**, 144409 (2002); M. C. Sánchez, G. Subías, J. García, and J. Blasco, Phys. Rev. Lett. **90**, 045503 (2003).

[7] J. M. Michalik, J. M. De Teresa, C. Ritter, J. Blasco, D. Serrate, M. R. Ibarra, C. Kapusta, J. Feudenberger, and N. Kozlova, Europhys. Lett. **78**, 17006 (2007).

[8] J. Rodríguez-Carvajal, Physica B **192**, 55 (1992); available at www-llb.cea.fr

[9] A. Filipponi, M. Borowski, D. T. Bowron, S. Ansell, A. DiCicco, S. de Panfilis, and J. P. Itiè, Rev. Sci. Instrum. **71**, 2422 (2000).

[10] B. Ravel and M. Newville, J. Synchrotron Radiat. **12**, 537 (2005).

[11] J. J. Rehr and R. C. Albers, Rev. Mod. Phys. **72**, 621 (2000).

[12] K. G. Bramnik, G. Miehe, H. Ehrenberg, H. Fuess, A. M. Abakumov, R. V. Shpanchenko, V. Yu Pomjakushin, and A. M. Balagurov, J. Solid State Chem. **149**, 49 (2000).

[13] P. M. Woodward, Acta Crystallogr., Sect. B: Struct. Sci. **53**, 32 (1997).

[14] J. Herrero-Martín, J. García, G. Subías, J. Blasco, and M. C. Sánchez, J. Phys.: Condens. Matter **16**, 6877 (2004).

[15] J. S. Stephens and D. W. J. Cruickshank, Acta Crystallogr., Sect. B: Struct. Crystallogr. Cryst. Chem. **26**, 222 (1970).

[16] A. J. Berry and H. St. C. O'Neill, Am. Mineral. **89**, 790 (2004).

[17] B. M. Weckhuysen, R. A. Schoonheydt, J.-M. Jehng, I. E. Wachs, S. J. Cho, R. Ryoo, S. Kijlstra, and E. Poels, J. Chem. Soc., Faraday Trans. **91**, 3245 (1995).

[18] Z. Zeng, I. D. Fawcett, M. Greenblatt, and M. Croft, Mater. Res. Bull. **36**, 705 (2001).

[19] C. Brouder, J. Phys.: Condens. Matter **2**, 701 (1990).

[20] A. Manceau, A. Gorshkov, and V. A. Drits, Am. Mineral. **77**, 1133 (1992).

[21] F. Farges, G. E. Brown, and J. J. Rehr, Phys. Rev. B **56**, 1809 (1997).

[22] T. E. Wesre, P. Kennepohl, J. G. DeWitt, B. Hedman, K. O. Hodgson, and E. I. Solomon, J. Am. Chem. Soc. **119**, 6297 (1997).

[23] Z. Y. Wu, D. C. Xian, T. D. Hu, Y. N. Xie, Y. Tao, C. R. Natoli, E. Paris, and A. Marcelli, Phys. Rev. B **70**, 033104 (2004).

[24] Y. Joly, D. Cabaret, H. Renevier, and C. R. Natoli, Phys. Rev. Lett. **82**, 2398 (1999).

[25] A. Magneli, Acta Crystallogr. **9**, 1038 (1956).

[26] G. Popov, M. Greenblatt, and M. Croft, Phys. Rev. B **67**, 024406 (2003).

[27] J.-H. Choy, D.-K. Kim, S.-H. Hwang, G. Demazeau, and D.-K. Jung, J. Am. Chem. Soc. **117**, 8557 (1995).

[28] J. Herrero-Martín, G. Subías, J. Blasco, J. García, and M. C. Sánchez, J. Phys.: Condens. Matter **17**, 4963 (2005).

[29] Z. Hu, H. von Lips, M. S. Golden, J. Fink, G. Kaindl, F. M. F. de Groot, S. Ebbinghaus, and A. Reller, Phys. Rev. B **61**, 5262 (2000).

[30] L. M. F. de Groot, Z. W. Hu, M. F. Lopez, G. Kaindl, F. Guillot, and M. Tronc, J. Chem. Phys. **101**, 6570 (1994).

[31] M. Roy, S. J. Gurman, and G. van Dorssen, J. Phys. IV **7**, 151 (1997).

[32] H. Taguchi, M. Nagao, and Y. Takeda, J. Solid State Chem. **114**, 236 (1995).

[33] R. D. Shannon, Acta Crystallogr., Sect. A: Cryst. Phys., Diffr., Theor. Gen. Crystallogr. **32**, 751 (1976).

[34] A. Kuzmin, J. Purans, G. Dalba, P. Fornasini, and F. Rocca, J. Phys.: Condens. Matter **8**, 9083 (1996).